Int J Mech Mater Des (2022) 18:491–507
https://doi.org/10.1007/s10999-021-09580-8

Dynamic response predictions of frictionally constrained lap joints subjected to cyclic loading

Seunghun Baek

Received: 4 August 2021 / Accepted: 9 November 2021 / Published online: 27 January 2022

Abstract We consider a simple frictionally constrained lap joint. Two identical beams were joined by a constant normal load. A periodic bending moment was applied on each beam to investigate the contact tractions at the joint interface. Predicting the dynamic behaviors of a frictionally constrained lap joint under periodic loading is challenging owing to the inherent nonlinearity of the behaviors. A dynamic response analysis of nonlinear systems is generally conducted via numerical integration in the time domain. However, owing to the nonlinear nature, time-domain analyses are computationally expensive. To address this issue, efficient reduced-order modeling (ROMs) was proposed in this paper. The proposed technique is based on the interpretation of the nonlinear characteristics of the friction force as relevant damping and stiffness terms. To increase the computation speed, the proposed method allows for the precalculation of the equivalent terms and employs response-dependent equivalent parameters in iterative solution methods. For validation, steady-state responses due to periodic bending were examined. The results obtained from the ROMs agree well with those of the time-domain analysis conducted using the full finite-element model. This study demonstrates that the equivalent expression of the nonlinear friction force can be defined by equating the energy loss or store per cycle in a hysteretic system to the energy loss or store per cycle in the corresponding amplitude. The proposed technique permits accurate predictions of the steady-state response of resonant vibrations in a primarily nonlinear hysteretic system.

Keywords Friction damping · Reduced order modeling · Structural vibration

1 Introduction

In several engineering applications, the dynamic behavior of assembled structures is influenced by the flexibility of joints. Microslips, which result in frictional energy dissipation, are observed in frictionally constrained joints subjected to dynamic loading. In general, damping resulting from the internal hysteresis of a material is low, and 90% of the damping in most structures occurs in structural joints (Beards 1983). Thus, the identification of damping associated with mechanical joints is crucial. The damping associated with mechanical joints is more dominant than that associated with other damping sources, such as material damping (Gaul and Nitsche 2001). This is particularly true for lightly damped flexible structures. Thus, the relevant physics of the joint should be

S. Baek (✉)
Pusan NU: Pusan National University Busan,
Busan Gwang'yeogsi, Republic of Korea
e-mail: baeksh@pusan.ac.kr

investigated for validating the dynamic response of the structure.

The dynamic behavior of structures is affected by external forces and friction at the interfaces of bolted, riveted, and compression joints. To increase and utilize inherent structural damping, the frictional damping between the structural joints should be well-understood and controlled. The mechanism of the friction arising from the mechanical joint interface is complicated because it is considerably influenced by the relative motion and interface load. For joints with a high normal interface pressure, mutual embedding of the surface may occur. In contrast, slip mechanisms tend to emerge with a low normal interface pressure. Thus, in all cases, the force and moment transfer mechanisms of the joints must be understood to design an efficient structure.

Empirical parametric studies on the design factors that influence the stiffness of mechanically fastened joints are expensive and time-consuming. Hence, a numerical study, which is economical, is preferred. Thus far, numerous studies have been conducted on frictionally constrained clamped joints. Den Hartog proposed an analytical approach for a dry friction damper system using a single-degree-of-freedom (SDOF) model (Den Hartog 1930). To access the exact solutions of the responses at the steady state, he used the piecewise linear characteristic of the Coulomb friction law. Similarly, multiple-DOF systems for clamped joints that exhibit local hysteretic behavior have been considered (Lotstedt 1982; Miller 1977; Pfeiffer 1991, 1992). Gaul and Nitsche (2001) examined various joint models, including their correlations to material plasticity. In addition, they presented a semi-active damping joint for vibration control applications. Mead and Eaton (1960) and Eaton and Mead (1963) theoretically and experimentally investigated the energy dissipation of a viscoelastic interfacial-layered lap joint. Earles (1966) proposed a theoretical method for estimating the energy dissipation by the friction force in a simple lap joint. A survey and research on dry friction were presented by Ferri (1995) and Beards (1983). Recently, Anothai Thaitirarot (2013) investigated the contact mechanisms of a frictional lap joint, focusing on the detailed nature of the contact traction between the laps of the joints. Kim and Jang (2014, 2017) numerically investigated frictional contact problems by subjecting two asymmetric objects to cyclic loading. The transitions of the contact status during the transient and steady states under cyclic loading were precisely studied. Similarly, Sabelkin and Mall (2006) investigated the interactions between deformable segments subjected to periodic loading and unloading. Several studies have employed the harmonic balance method (HBM) or similar methods to predict the response of frictionally constrained joints (Ren et al. 2008; Ahmadian and Jalali 2007; Lacayo and Pesaresi 2019). The analysis time of frequency-domain techniques using the HBM is considerably lower than that of the time-domain analysis techniques. However, the computational cost is proportional to the number of governing equations involved in nonlinearity. Therefore, model reduction methods have been proposed to reduce the computational costs of structural problems (Nickell 1976; Noor 1981; Bathe and Gracewski 1981). Slaats et al. (1995) developed optimal reduction techniques using a set of basis vectors. They selected vectors at a specific time instant to construct the basis vectors. Wu and Tiso (2016) proposed an efficient ROM method that refines the classical linear reduction based on modal derivatives. Witteveen and Fischer (2014) and Pischler et al. (2017, 2017) presented effective and advanced model reduction methods. The flexibility within the joint area was captured by extending the reduction base, which consisted of special joint trial vectors. Their approaches allowed for the investigation of nonlinear contact and friction forces at joint interfaces. They exhibited outstanding performance for estimating the responses of joint systems in the time domain, providing accurate investigations of the nonlinearities in the joint in terms of contact and friction forces. Recently, Areias et al. (2020) proposed an efficient two-stage contact algorithm by introducing three additional DOFs corresponding to the contact forces. This technique was proven to be effective for predicting stick-slip behavior. However, this approach is applicable solely for quasi-static cases.

Determining the influence of force and excitation frequency on the motion of a system is crucial for engineering applications. Moreover, the variations in material properties that induce the nonlinear behavior of systems are crucial from the perspective of structural design. The analysis of the dynamic response of nonlinear structures in the relevant frequency range is often time-consuming, particularly for obtaining the responses at the steady state. To address this problem,

ROM was proposed in this paper. An efficient technique for predicting the steady-state response of a simple lap joint subjected to a nonlinear force was presented. The ROM technique is constructed according to a transformation matrix, which comprises normal modes from two different contact interface conditions to describe the relative displacement of contact pairs. The underlying idea of this reduction method is to express the nonlinear friction forces at the contact interface as piecewise linear response-dependent functions. The contact friction force was precalculated quasi-statically using finite element modeling (FEM). The resulting energy dissipation is replaced by the expressions for the equivalent damping and stiffness. Then, the governing equation, which forms a set of algebraic equations, is solved using an iterative method. The ROM technique is not time-consuming; that is, the technique considerably reduces the computational time required. The proposed ROM technique was validated by comparing its predictions of forced responses with those obtained via the time-domain analysis (TDA) conducted using a full FE model.

2 Methodology

In this section, a simple lap-joint FE model and the boundary conditions are discussed. We considered a simple two-dimensional (2D) frictional lap joint, in which two overlapping flat plates were constrained by frictional contact, and the boundary of each plate was subjected to a bending moment. Appropriate boundary conditions with spring elements allow for the modeling of the contact surface with an arbitrary load transfer. The overall contact interface was assumed to obey the Coulomb friction, and the commercial FE package ANSYS was employed for the FE modeling and for obtaining the numerical solution.

2.1 Lap joint modeling

The single-lap joint modelled in this study is shown in Fig. 1. The joint comprises two identical beams of length L, which overlap by a distance of $2L_o$ and are bound together by a normal load P distributed over the range of $2L_p$. In this lap-joint model, the following conditions were considered.

- The geometry is strictly 2D; thus, the longitudinal cross section of the beam cutting across the center of the width is considered.
- The effect of bolting is accounted for by the constant clamping force P uniformly distributed over L_P.
- The time-varying bending moment $M(t)$ is introduced at the joint ends.
- The bending moment that bends the beam concave upward is considered to be positive.
- Only the vertical transverse displacement at the two unjointed ends is constrained to be zero.
- Both of the joints have symmetry conditions along the joint edges.

Numerous engineering joint applications were subjected to periodic or repetitive loading, resulting in energy dissipation at the contact interfaces, which added damping to the system. This study primarily explored the effect of dry friction damping when a joint undergoes periodic loading. The load transfer in the joint was characterized by the normal load P and the bending moment $M(t)$. The time-varying bending moment is described as follows:

$$M(t) = M_o sin(\omega t) \tag{1}$$

where M_o is the magnitude of the bending moment; ω is the excitation frequency; and t is the time.

An FE model was obtained using the commercial FE analysis program, ANSYS. PLNAE182 was used to construct a beam element. This element exhibits the potential for modeling 2D solid structures with two DOFs, $x - y$ directions, at each node; further, this element exhibits plasticity and stress stiffening as well as geometric nonlinearity, including large deflection and strain. For the contact interface, the surface-to-surface elements CONTA172 and TARGE169 were selected. These elements are applicable to 2D structures and allow for a deformable surface at the contact interfaces. Contact was detected when one surface penetrates the other surface. In addition, the element PLNAE182 allows for separation, bonding, and interface delamination.

The FE mesh modeling is shown in Fig. 2. To improve the computational efficiency, the mesh sizes were controlled for three different regions: contact interfaces, overlapping portions, and the rest of the elements. To achieve an accurate numerical analysis, a high density mesh was employed at the contact

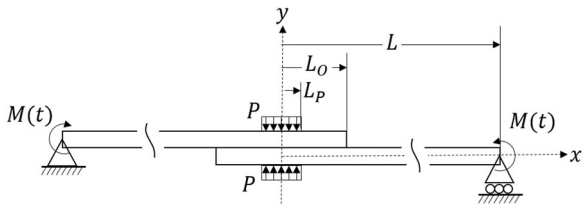

Fig. 1 Schematic of the lap-joint model

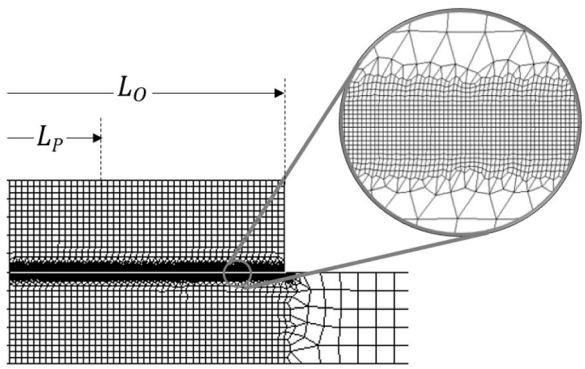

Fig. 2 Lap-joint FE model

interface. The size of the mesh n was controlled by varying the number of contact pairs J distributed over the length of the contact interface L_o.

In Fig. 3, the convergence of energy dissipation with respect to the mesh size is shown. The material density was $2g/cm^3$, and the Young's modulus was 70 GPa. To make the damping effect from the friction force dominant, a low material damping was adopted. Damping was controlled by applying Rayleigh damping. α and β were the constants of the proportionality of Rayleigh damping, and the values were selected as $\alpha = 0$ and $\beta = 7.3 \times 10^{-7}$, which correspond to a damping ratio $\zeta = 3.9 \times 10^{-4}$ at $\omega_n = 170Hz$. The friction coefficient was set to $\mu = 0.25$, which resulted in a maximum friction force of 0.25 when it was normalized by the pressure P. The friction force calculated from the finite element model may vary depending on the normal load and relative motion between the contact interfaces. The relative motions were significantly affected by the mesh size owing to geometric nonlinearity and element penetration. At the given geometry, boundary conditions, and model parameters, a proper mesh size control can guarantee the convergence of the resulting relative motion at the joints. In this study, the geometry, boundary conditions, and model parameters were fixed to ensure a consistent model accuracy. Solely the external excitation frequency and friction coefficients are the parameters of engineering design. The dissipated energy ΔE_{act} per cycle by the friction force F_f was computed in the steady state as $\Delta E_{act} = \sum_{j=1}^{J} \int_D F_{fj} dx_j$, where j is the index of the

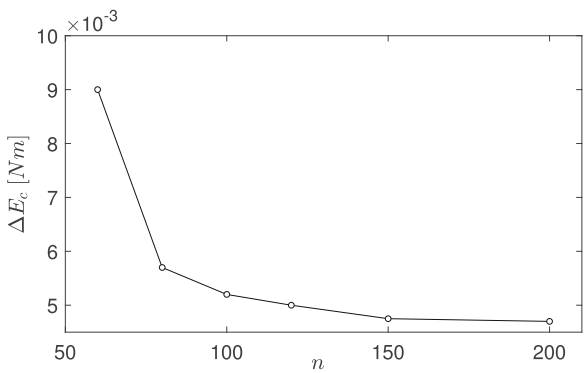

Fig. 3 Energy dissipations for different mesh sizes at $M_o/L = 0.0167$, $\omega = 170Hz$

contact pair. The dissipated energy at the steady state decreased sharply until $n = 80$ and started to converge at $n = 150$ with a relative error of less than 1%. The relative error between $n = 150$ and $n = 200$ was approximately 0.106%. In this study, the mesh size was selected as $n = 200$.

2.2 Contact modeling

The FE model is flexible, and the contact interface comprises a discrete contact point. According to the penalty-based method and the tangential Coulomb friction force, the contact element can provide compression in the direction normal to the contact surfaces. Contact kinematics are crucial for evaluating the effective damping and stiffness of the friction interface because the contact behavior induced by the friction force is exclusively identified by the relative motions of the contact interface. The two components comprising the contact kinematics are illustrated in Fig. 4). The tangential component k_t helped determine the stick/slip of the contact, and the normal component k_n caused normal load variations.

According to the contact normal force p and shear force f at a contact node pair, the contact is classified into one of the following four states:

Stick	$p \geq 0,$	$\lvert f \rvert \leq \mu p,$	$\dot{x} = 0$
Forward slip	$p \geq 0,$	$f = -\mu p,$	$\dot{x} > 0$
Backward slip	$p \geq 0,$	$f = \mu p,$	$\dot{x} < 0$
Separation	$p = 0,$		$y > 0$

2.3 Definition of equivalent damping and stiffness

Consider the EOMs for a lap joint system comprising r DOFs, including nonlinear friction interfaces:

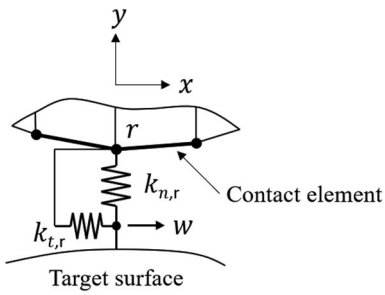

Fig. 4 Contact modeling, where $k_{t,r}$ and $k_{n,r}$ represent stiffness in the tangential and normal direction, respectively

$$\mathbf{M}\ddot{\mathbf{x}}(t) + \beta\mathbf{K}\dot{\mathbf{x}}(t) + \mathbf{K}\mathbf{x}(t) + \mathbf{F}_f(\mathbf{x}(t), \dot{\mathbf{x}}(t)) = \mathbf{F}(t), \tag{2}$$

where the $(r \times 1)$ vector $\mathbf{x}(t)$ contains the DOF of the system. The $(r \times r)$ matrices $\mathbf{M}$ and $\mathbf{K}$ represent the mass and stiffness. The $\mathbf{K}$ matrix is the stiffness matrix defined by the sliding state, in which all the tangential constraints in the interfaces are removed. $\mathbf{F}$ is the $(r \times 1)$ vector of external harmonic force with an excitation frequency of ω, and $\mathbf{F}_f$ is the $(r \times 1)$ vector of the contact friction forces. The Rayleigh damping ratio was set to $\alpha = 0$ and $\beta = 4.44 \times 10^{-6}$ s.

Local relative motions between the contact interfaces were allowed because FE modeling is flexible. Therefore, the relative displacements at the friction contact were inevitably nonconstant. Interaction forces as well as stiffness properties due to abrupt changes in the contact condition also developed discontinuously. However, for a system exposed to harmonic excitations, the contact friction may reach a characteristic cycle at a steady state. The principal assumption of a steady-state analysis was that the motion of the system is symmetrical for each half-cycle. This assumption allows for the consideration of the displacement from the positive maximum to the negative maximum only (Beucke and Kelly 1985). Based on the assumption that the response of the structure is harmonic, the steady-state response of the system can be described as follows:

$$\mathbf{x}(t) \approx \mathbf{X}sin(\omega t) \tag{3}$$

where $\mathbf{X}$ is the $(r \times 1)$ vector of the amplitude of the motion in the steady state. Moreover, in several cases, the steady-state amplitude of harmonic motion is expressed by employing only the principal harmonic (Allara 2009; Baek and Epureanu 2017).

$$\mathbf{X} = \mathbf{\Phi}q = [\,\mathbf{\Phi}_{sl} \quad \mathbf{\Phi}_{st}\,]q \tag{4}$$

where the $(r \times 1)$ vector $\mathbf{\Phi}_{sl}$ is the normal mode shape of the lap joint under the full sliding condition at the contact interface, $(r \times 1)$ vector $\mathbf{\Phi}_{st}$ is the normal mode shape where the relative motion is limited to the contact pairs, and q is the modal amplitude.

The underlying principle of the proposed method was to postulate the equality of the friction force by the equivalent damping force and elastic force during the excitation cycle. If the exact friction force can be obtained, no additional assumption is required to

calculate the dissipated energy per cycle. Therefore, a quasi-static analysis was conducted to compute the friction force at the contact surface. The resulting friction force $\mathbf{F}_f$ can be obtained by introducing the motion given in Eq. (3) . Thus, the total amount of energy dissipation can be computed as follows:

$$\begin{aligned}\Delta E_{act} &= \int_D \mathbf{F}_f d\mathbf{x} \\ &= \int_T \dot{\mathbf{x}}^T \mathbf{F}_f dt \\ &= \int_T \omega q \mathbf{\Phi}^T \mathbf{F}_f cos(\omega t) dt \\ &= q \int_0^{2\pi} \mathbf{\Phi}^T \mathbf{F}_f cos\theta d\theta \\ &= q W_c.\end{aligned} \tag{5}$$

Equivalently, the energy dissipation per cycle at a steady state was computed by assuming harmonic motion. Without calculations of the exact solution, the motion was assumed to be harmonic at the steady state to compute the energy loss per cycle.

$$\begin{aligned}\Delta E_{eq} &= \pi \gamma_{eq} \mathbf{X}^T \mathbf{K} \mathbf{X} \\ &= \pi \gamma_{eq} q \mathbf{\Phi}^T \mathbf{K} \mathbf{\Phi} q \\ &= \pi \gamma_{eq} \omega_n q^2.\end{aligned} \tag{6}$$

where γ_{eq} is the equivalent structural damping factor. The energy dissipation derived from Eq. (5) and the relevant expression given in Eq. (6) are equivalent. Hence, the equivalent damping can be obtained as

$$\gamma_{eq} = \frac{W_c}{\pi \omega_n q}. \tag{7}$$

When the shear force was small, the induced friction forces did not exceed the slip load; thus, the contact surface was fully stuck. During this stick state, the tangential friction force was induced by elastic asperity deformation (Petrov and Ewins 2003). The variation in the elasticity at the contact surfaces (k_t) added more strain energy to the system. Therefore, the friction force, which was in phase with the displacement, affected the resonance of the lap joint system. The average elastic energy due to the friction force $\mathbf{F}_f$ during a cycle can be computed as

$$\begin{aligned}\Delta \bar{E}_{act} &= \frac{1}{T} \int_T \mathbf{x}^T(t) \mathbf{F}_f dt \\ &= \frac{\omega}{2\pi} \int_T q \mathbf{\Phi}^T \mathbf{F}_f sin(\omega t) dt \\ &= \frac{1}{2\pi} q \int_0^{2\pi} \mathbf{\Phi}^T \mathbf{F}_f sin\theta d\theta \\ &= \frac{1}{2\pi} q W_s.\end{aligned} \tag{8}$$

Similarly, the average stored energy associated with the tangential friction stiffness at the frictional contact during the excitation period can be obtained as

$$\begin{aligned}\Delta \bar{E}_{eq} &= \frac{1}{T} \int_T (\mathbf{K}_e \mathbf{x}(t))^T \mathbf{x}(t) dt \\ &= \frac{1}{T} \int_T q \mathbf{\Phi}^T \mathbf{K}_e \mathbf{\Phi} q sin^2(\omega t) dt \\ &= \frac{\omega}{2\pi} \int_0^{2\pi} q^2 k_e sin^2\theta \frac{d\theta}{\omega} \\ &= \frac{1}{2\pi} k_e q^2.\end{aligned} \tag{9}$$

where $\mathbf{K}_e$ is the $(r \times r)$ effective stiffness matrix associated with the tangential friction stiffness. The average elastic energies defined in Eq. (8), and the stored energy on average, as described in Eq. (9) are equal. Thus, the equivalent stiffness can be expressed as

$$k_{eq} = \frac{W_s}{q}. \tag{10}$$

The friction forces considered for energy dissipation were investigated only in the steady state. Thus, the equivalent damping and stiffness defined in Eqs. 7 and 10, respectively, were constant for a given force condition. Based on this idea, the friction force was linearized by the equivalent stiffness and damping in the reduced-order space.

2.4 Reduced order modeling

In general, by solving the governing equation in Eq. (2) with full-order models is challenging owing to the size of the models and the nature of the nonlinear force. Hence, effective model reduction is required to abate the computational efforts to study the dynamic characteristics of the lap joint. The key idea of the reduction is to predict the resulting friction force by

capturing the relative motion. The nonlinear friction force is localized at the contact DOFs, and these contact DOFs are a considerably smaller in number than the rest of the lap-joint DOFs. A recent study by Dossogne et al. (2017) demonstrated that most of the energy dissipation occurs when the pressure is low, which is a regime that is away from the bolted joints. This indicates that the response data within the prestressed region or in the vicinity of the prestressed region should include relative motions.

To capture the relative motions, two linear systems can be considered by manipulating the constraints in the contact interfaces: full sliding and sticking. If all constraints in the tangential motion of the contact interface are removed, the joint can slide freely without any energy loss. This full sliding system motion can be captured by its normal mode, $\mathbf{\Phi}_{sl}$. By bonding the contact pairs within the prestressed region of the full sliding system, the relative motions within and in the vicinity of the prestressed region are restricted. Such a linear system can also be represented by the normal mode $\mathbf{\Phi}_{st}$. The forced response associated with friction and its contact status can retain the intermediate state between the full sticking and limited sliding. The resulting contact interface motions are well-captured by the combination of $\mathbf{\Phi}_{sl}$ and $\mathbf{\Phi}_{st}$. A similar idea was applied by Chen and Menq (1998). In his paper, the concept of hybrid modes was proposed to investigate the frictionally constrained system. The hybrid modes comprise two different modes: free and constrained modes. The free mode is the normal mode free from the frictional constraint, and the constrained mode is obtained by restricting the contact DOFs. Tang and Epureanu (2019) and Tang et al. (2017) also adopted a relevant idea to estimate the dynamic response of frictionally constrained blisks. He presented a set of mode bases to predict the forced responses of frictional contact, introducing a normal mode with gross slip at the contact DOFs and the other normal mode by constraining the relative motions at the contact interfaces.

Considering the assumption discussed above, the motion of a lap joint $\mathbf{X}$ is projected onto a modal basis using the following transformation:

$$\mathbf{X} = \begin{bmatrix} \mathbf{\Phi}_{sl} & \mathbf{\Phi}_{st} \end{bmatrix} \begin{bmatrix} q_{sl} \\ q_{st} \end{bmatrix} = \mathbf{T}\mathbf{q}, \tag{11}$$

where $\mathbf{T}$ is the $(r \times 2)$ transformation matrix, and $\mathbf{q}$ is the (2×1) modal amplitude vector, which comprises the modal amplitude q_{sl} and q_{st}, corresponding to $\mathbf{\Phi}_{sl}$ and $\mathbf{\Phi}_{st}$, respectively.

By introducing the transformation matrix $\mathbf{T}$ into Eq. (2), the governing equation can be written as follows:

$$\left[-\omega^2\mathbf{m} + (i\omega\beta\ + 1)\mathbf{k}\right]\mathbf{q} + \mathbf{f}_f = \mathbf{f}, \tag{12}$$

where

$$\mathbf{m} = \mathbf{T}^T\mathbf{M}\mathbf{T} = \begin{bmatrix} 1 & \mathbf{\Phi}_{sl}^T\mathbf{M}\mathbf{\Phi}_{st} \\ \mathbf{\Phi}_{st}^T\mathbf{M}\mathbf{\Phi}_{sl} & 1 \end{bmatrix}, \tag{13}$$

and

$$\mathbf{k} = \mathbf{T}^T\mathbf{K}\mathbf{T} = \begin{bmatrix} \omega_n^2 & \mathbf{\Phi}_{sl}^T\mathbf{K}\mathbf{\Phi}_{st} \\ \mathbf{\Phi}_{st}^T\mathbf{K}\mathbf{\Phi}_{sl} & \mathbf{\Phi}_{st}^T\mathbf{K}\mathbf{\Phi}_{st} \end{bmatrix}. \tag{14}$$

Note that ω_n is the natural frequency of the lap joint without a friction force at the contact interfaces. As addressed in the previous section, the nonlinear friction force was replaced by the linearized term of damping and stiffness, which functions as the modal amplitude q_l. The friction force projected onto the modal basis is expressed as follows:

$$\mathbf{f}_f = \left(i\gamma_{eq}(q_{sl}) + k_{eq}(q_{sl})\right)\mathbf{I}\mathbf{q}. \tag{15}$$

Substituting Eq. (15) into Eq. (14), the reduced model EOMs for the lap joint are as follows:

$$\underbrace{\left[-\omega^2\mathbf{m} + (i\omega\beta\ + 1)\mathbf{k} + \left(i\gamma_{eq}(q_{sl}) + k_{eq}(q_{sl})\right)\mathbf{I}\right]}_{\mathbf{\Theta}^{-1}}\mathbf{q} = \mathbf{f}. \tag{16}$$

Although the receptance matrix $\mathbf{\Theta}$ carries response-dependent components $\gamma_{eq}(q_{sl})$ and $k_{eq}(q)$, they are precalculated prior to the ROM processes, providing rapid assessments. At a particular excitation frequency ω, the following iterative algorithm can be used:

$$\mathbf{q}_{i+1} = \mathbf{\Theta}_i\mathbf{f} \tag{17}$$

where $\mathbf{q}_{i+1}$ denotes the solution vector at the $(i+1)^{\text{th}}$ iteration step, and $\mathbf{\Theta}_i$ is the receptance matrix at the iteration step i. The iterations continue until the relative error of the solution between the current and the previous step $e = ||\mathbf{q}_{i+1} - \mathbf{q}_i||/||\mathbf{q}_i||$ converges below ε.

3 Results

In this section, the idealized lap-joint model is analyzed to investigate the force transfer, contact behavior, and energy dissipation at the contact surface. A bending moment was introduced at the end of the laps in the form of cyclic loading, as described in Eq. (1) and was repeatedly applied until a steady state was attained. The assessment of the interfacial characteristics of the contact behavior was conducted for both quasi-static and dynamic analyses.

First, nonlinearity of the contact motions induced by bending moments was quasi-statically explored. Static analysis was performed as follows: Initially, normal pressure P was applied to the clamping area, and system equilibrium was obtained. In this step, the contact interfaces were assumed to be frictionless so that the memory effect of the friction force is removed. Next, a periodic moment $M(\theta) = M_o sin(\theta)$ was applied at the end of the joints, and the contact forces were computed quasi-statically by incrementing θ. To attain a reliable numerical resolution, 150 step sizes per loading period were adopted. When the loading cycle was completed, the same procedure was repeated, and the magnitude of M_o was updated from the initialized equilibrium. The transition of the contact states, normalized contact pressure $\mu p(x)/P$, and normalized tangential traction $f(x)/P$ distributions are depicted in Fig. 5. The contact states for the stick, forward slip, backward slip, and separation are indicated as 1, 2, 3, and 4, respectively. When prestress was applied under normal pressure, the contact ranged in length of $\pm 1.18L_P$. Under prestress, all the contacts belong to the stick region. As bending was applied in the positive direction, where the joint bends concave up, contact develops unsymmetrically. At the maximum positive bending moment, the left-hand side contact contracts to $-1.12L_P$ whereas the right-hand side contact expands to $1.29L_P$. The contact pressure and tangential traction distribution at $M(\theta) = M_o$ are shown in Fig. 5b). The transitions between the forward and backward slips occur at the maximum magnitude of the moment. As the moment decreased further and reached 0, the contact distribution recovered its initial region. Additionally, the contact pressure decreased to its initial distribution. The shear traction remained a locked-in distribution at the outer contact edges. ($M(\theta) = 0$ in Fig 5b). At $M(\theta) = -M_o$, the contact increased to $-1.29L_P$ and $1.12L_P$. The contact traction distributions at $M(\theta) = -M_o$ are demonstrated in Fig. 5b). The nonlinear interaction of the contact surface enters the steady-state solution during the second loading cycle. Upon reapplication of the bending moment, the forward slip region shrinks, but the backward slip region remains the same or widens. The detailed normal pressure distributions and tangential contact traction are shown in Fig. 5c. When the bending moment amplitude is increased, the slip regions increase, and this determines the relative motion modal amplitude q.

Next, the contact pressure and shear traction at the contact interfaces for each loading cycle were investigated in the time domain. For time-domain analysis, the time step size Δt is defined by $\Delta t = 1/(N_s f_{ex})$, where f_{ex} is the excitation frequency and N_s is the number of time steps. In Fig. 6, the system responses in the time domain obtained from different sizes of N_s are shown. As observed, the analysis results start to converge when N_s is greater than 120. In this study, each loading cycle was solved in 150 increments to accurately capture the evolution of the contact region with stick/slip transitions. The steady state was determined by computing the energy-dissipation convergence. After 180 cycles, the relative error of the dissipated energy between consecutive cycles converged to 1 The relevant quasi-static analysis was generated by applying a proper magnitude of the bending moment to induce the same level of slip ($q = 0.12$). In Fig. 7a, the evolution cycles of the contact states in the steady state are illustrated for both dynamic and static analyses. Here, we observe close alignments of the contact boundaries and the evolution of stick-slip regions between the analyses for the two different domains. However, they may contain different distributions of contact traction. For instance, shear traction f in Fig. 7c shows a sudden decrease and recovery near the boundary of the forward slip ($\mu p = f$) and stick ($\mu p > f$) whereas the results obtained from the quasi-static analysis (Fig. 7b) indicate the smooth transitions in the same region.

The pressure smoothly disappears at the boundary of the contact, and the slip velocity decreases to 0 at the edge of the stick; hence, the maximum slip can be found at an intermediate point within the slip area. However, the global distributions of frictional slip within the slip region may differ between the two analyses, and this contributes to the generation of dissimilar energy dissipation in the slip region. For the

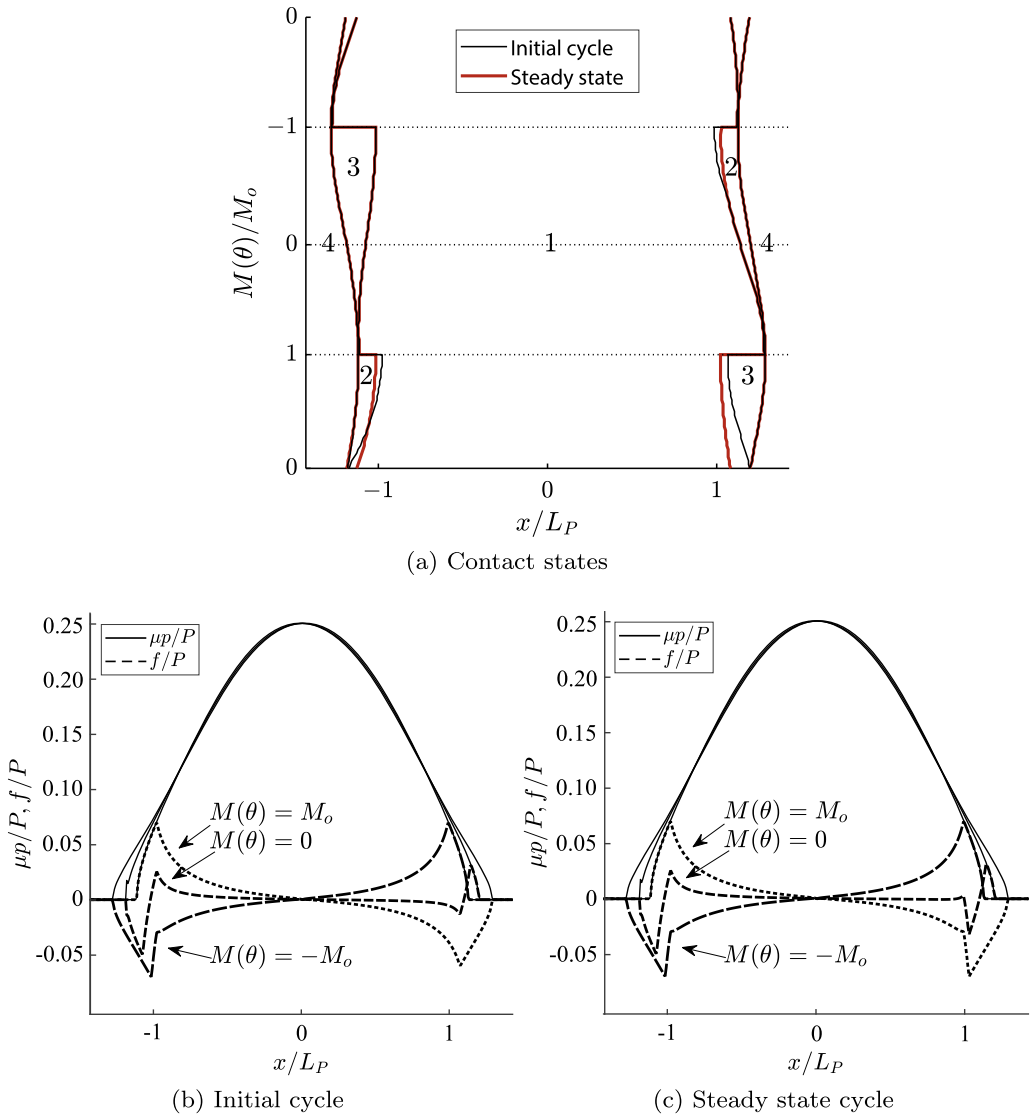

(a) Contact states

(b) Initial cycle

(c) Steady state cycle

Fig. 5 Interfacial tractions from quasi-static analysis. **a** Evolution of four contact states. **b** Distributions of $\mu p/P$ and f/P during the initial loading cycle. **c** Distributions of $\mu p/P$ and f/P in the steady-state loading cycle

problem considered, the energy dissipation over the steady state period is illustrated in Fig. 8a. The energy dissipation is localized and has a peak value in an intermediate slip region; however, the location and magnitude of the peak value as well as the overall profiles for each analysis differ. Although there are pointwise distinctions between the two results, the assessment of the contribution of the frictional contact to the system must be quantified at the system level. The integrated energy dissipation, which is the area in the hysteresis loop in Fig. 8b, is extremely close for both analyses ($\approx 0.18 \times 10^{-3}$). The overall influence of the friction contact, characterized by the energy dissipation ΔE_{act} and the average stored energy $\Delta \bar{E}_{act}$, is described in the next section.

3.1 Equivalent damping and stiffness

As explored in the previous section, the characteristics of the contact behavior are quantified as the dissipated energy and average stored energy, and are indicated by Eqs. (5) and (9), respectively. The values obtained from the quasi-static and dynamic analyses are shown in Fig. 9. For efficiently generating the data point of

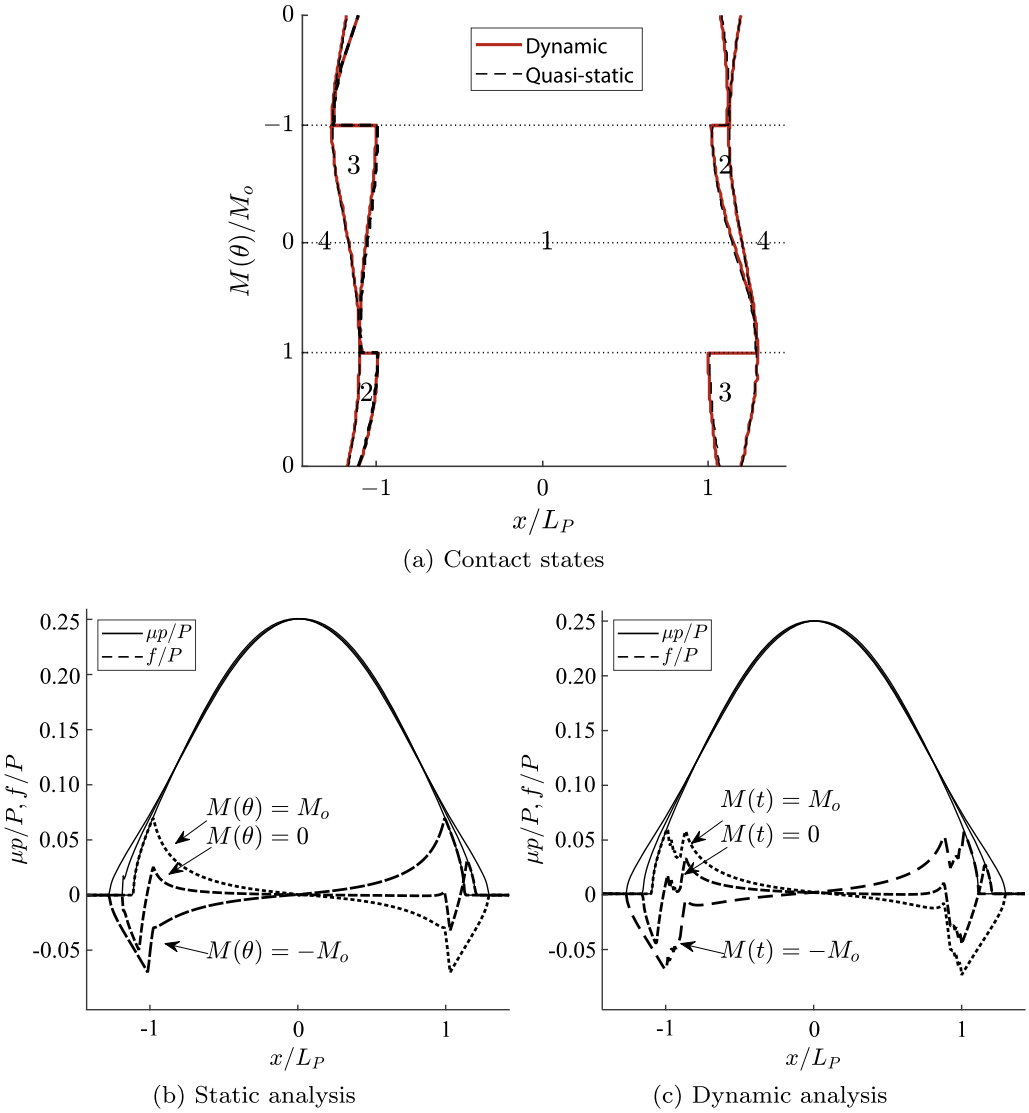

(a) Contact states

(b) Static analysis

(c) Dynamic analysis

Fig. 6 Nodal displacement in x-direction in time domain with different time step size (N_s). The node is examined at $x = L_p$

dynamic analysis, a smaller frequency spacing is employed near the resonance (175 *Hz*), but larger frequency step sizes are used in regions away from the resonance frequency. ΔE_{act} and $\Delta \bar{E}_{act}$ increase with an increase in the excitation frequency until they reach their maximum at the resonance frequency. These values then decrease as the excitation frequency increases beyond the resonance frequency. The effects of frictional contact, ΔE_{act}, and $\Delta \bar{E}_{act}$ evolve more rapidly when the excitation frequency approaches the resonant frequency from a lower frequency than from a higher frequency. This nonlinear behavior of the excitation frequencies contributes to unsymmetrical profiles of forced responses when a frequency sweep is introduced. The values of ΔE_{act} and $\Delta \bar{E}_{act}$ obtained via quasi-static analysis are shown as a solid line in Fig. 9. Discrepancies are observed between the results of the two analyses. The maximum relative errors are 3.6% for ΔE_{act} and 3.9% for $\Delta \bar{E}_{act}$ at 177*Hz*. The dynamic behavior of the contact tractions and variations in the normal force may not be equivalently projected in the static analysis results. Thus, the contributions of the contact tractions and stick/slip transitions at the friction interface under dynamic analysis can differ

from those under static analysis. However, the overall assessment of the effect of the contact behavior corresponding to the amplitude exhibited good correlations.

Figure 10 shows the evolution of the equivalent damping and stiffness relative to the modal amplitude q. The equivalent damping and stiffness are formulated according to Eqs. (7) and (10). The evolution of contact status between stick and slip can reduce the equivalent stiffness as the modal amplitude increases. The maximum modal damping occurs when the amplitude q lies between 0.05 and 0.1. This can be found in typical friction systems whose maximal damping efficiency is attained at the partial slip. Equivalent damping and stiffness assess the nonlinear friction force at each iteration of the solution method, forming the EOMs in Eq. (16) as a piecewise linear equation. Precalculation of γ_{eq} and k_{eq} prior to the process of the ROM ensures a computation speed in the order of seconds.

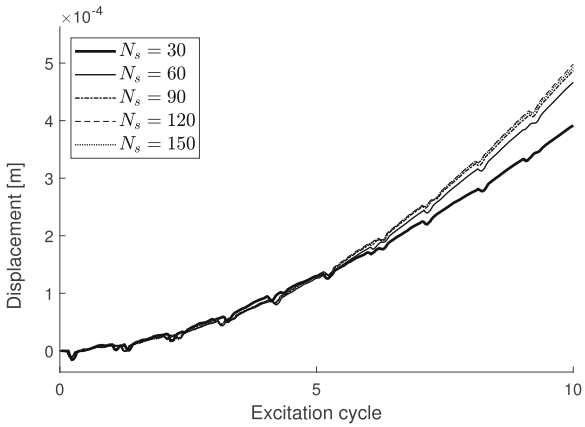

Fig. 7 Interfacial tractions at the steady state. **a** Evolution of four contact states. **b** Distributions of $\mu p/P$ and f/P from static analysis, resulting in $q = 0.12$ when $M_o/L = 0.03$. **c** Distributions of $\mu p/P$ and f/P from the dynamic analysis resulting in $q = 0.12$ when $f_{ex} = 174Hz$

3.2 Forced response prediction

The developed ROM was validated by comparing the forced responses obtained from the ROM and the full-size FE model. In Fig. 11, the forced responses in the modal coordinate along with the excitation frequencies are shown. The forced responses, that is, the solutions to Eq. (16), were obtained by the fixed-point iteration, as described in Eq. (17). The convergence of the fixed-point method is not always guaranteed and relies heavily on the receptance matrix and the choice of the initial approximation. However, a sufficiently close initial approximation may be advantageous to its solution. The converged solution of Eq. (16), which is

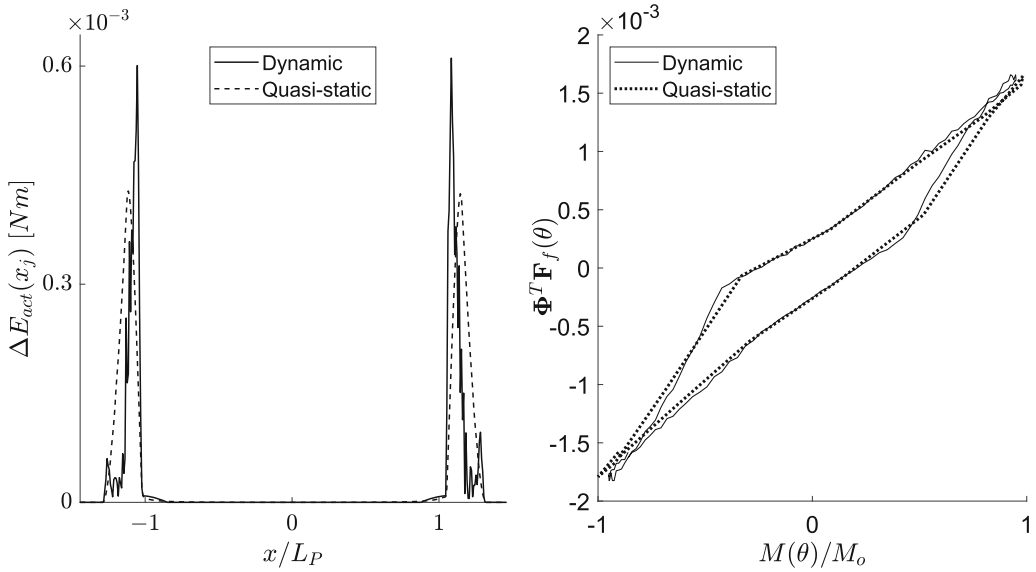

Fig. 8 Energy dissipation and hysteresis loop per cycle at the steady state

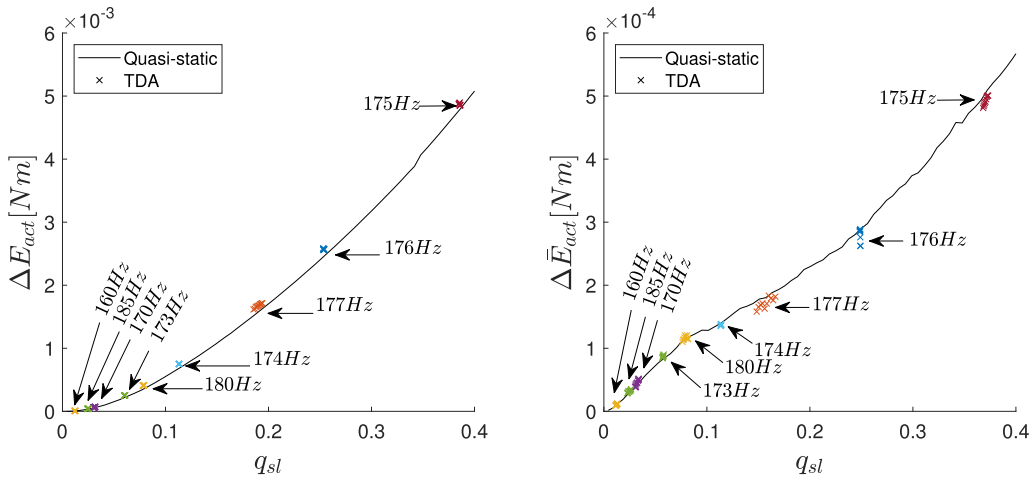

(a) Energy dissipation (b) Average stored energy

Fig. 9 Calculation of the **a** dissipated energy **b** average stored energy at the contact surface via static analysis and TDA

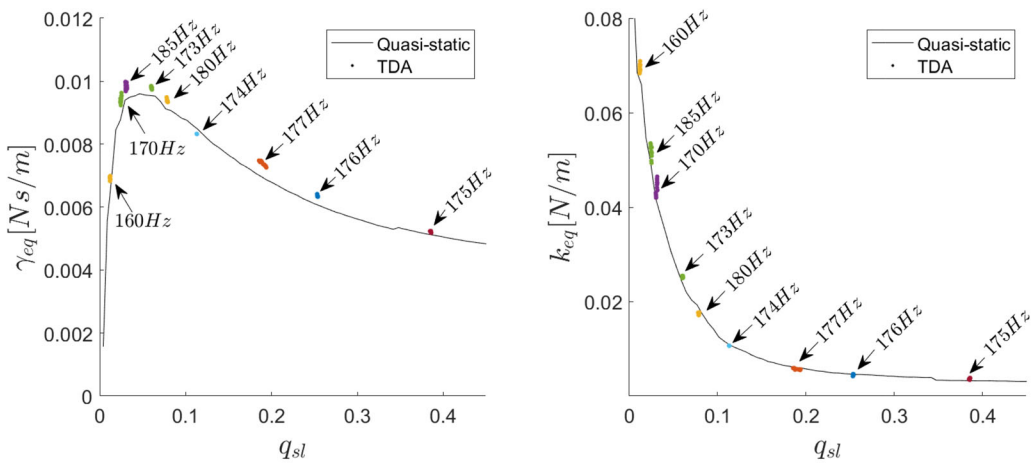

(a) Equivalent damping γ_{eq} (b) Equivalent stiffness k_{eq}

Fig. 10 TDA of **a** equivalent damping **b** equivalent stiffness as results of the ROM at each excitation frequency

generally obtained from excitation frequencies away from ω_n, can be adopted as an initial approximation of the neighboring excitation frequency. The incremental size of the excitation frequency can be chosen until the initial approximation satisfies the convergence of the solution. A detailed description of the convergence condition of the iterative solution of Eq. (16) can be found in "Appendices 1 and 2".

To explore the relative influence of the magnitude of the applied force, contact pressure, and friction coefficient on the system response, the ratio between the parameters $\rho = \frac{\mu PL}{M}$ is introduced. The first example includes forced response analyses of lap joints without a friction force at the contact interface ($\rho = 0$). The frictionless sliding condition at the frictional contact is modeled by setting $\mu = 0$ in this example. In the absence of a nonlinear friction force, the EOMs of ROM in Eq. (16) involve a general harmonic analysis as follows:

$$\left[-\omega^2\mathbf{m} + (i\omega\beta\ + 1)\mathbf{k}\right]\mathbf{q} = \mathbf{f}, \tag{18}$$

Furthermore, the forced response predictions indicated excellent agreement with the analysis results from ANSYS. When ρ increased to 0.8, the contact

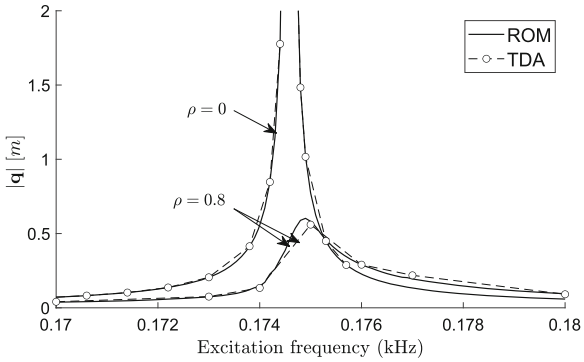

Fig. 11 Magnitude of modal amplitude **q** at each forcing frequency

friction force significantly affected the system. The maximum forced response decreased by approximately 90%, and the resonance frequency shifted from 174.6 to 174.9*Hz*. The relative errors between the predictions from the ROM and validation data from ANSYS were 0.8% near the natural frequency. Such a small error near the natural frequency indicates that the nonlinear contact behavior represented by the energy dissipation and stiffening is accurately captured. A maximum relative error of approximately 11% was observed at 177 *Hz*. The prediction errors are predominantly due to erroneous predictions of equivalent damping and stiffness.

Additionally, while maintaining guaranteed accuracy, the proposed ROM drastically reduced the computation time. For example, the time to compute a steady-state response in the time domain was 23 h 14 min. However, the overall response predictions within the frequency of interest took less than 15 s with an additional 10 min for the quasi-static analysis process. Notably, the additional time cost for quasi-static analysis was the entire time spent for repeated quasi-static computation. Thus, the quasi-static analysis time expense varied depending on the number of data points used to examine the equivalent stiffness and damping.

The nonlinear terms predicted by the ROM at each excitation frequency are specified. In Fig. 12, the resultant damping and stiffness values at each excitation frequency are shown for $\rho = 0.8$. There are discrepancies between the actual values obtained from the dynamic analysis in Fig. 10 and the prediction results from the ROM; however, the magnitudes and tendencies of the equivalent damping and stiffness along the excitation frequency were well-simulated with good agreement (Fig. 11). For example, higher accuracy was obtained near the resonance frequency. The relative errors at 175*Hz* were approximately 1% for the equivalent damping and 0.25% for the equivalent stiffness.

Owing to its efficient computations and high fidelity provided by the ROM, it enabled the characterization of the overall behavior of the lap joint for different ρ values. First, the resonance frequency increased with ρ. At a high level of ρ, the portion of the slip region during a loading cycle decreased, and this resulted in an increase in the stick portion, adding to the equivalent stiffness of the system. Second, the normalized response amplitude decreased with an increase in ρ owing to the development of equivalent damping. The damping effect lasted until it reached its optimal value ($\rho \approx 2.4$) and gradually diminished with an increase in ρ (Fig. 13).

These typical phenomena of a harmonic nonlinear response function with stiffening can be interpreted by the predicted damping and stiffness, as illustrated in Fig. 14). The predicted γ_{eq} and k_{eq} values are shown with respect to ρ and the excitation frequency. In general, at low ρ, where a relatively large amount of slip is allowed, a higher equivalent damping is generated; however, maximum damping does not occur at the resonance frequency each time. For instance, the maximum damping values and resonances are aligned only when ρ is close to 2.4. Likewise, k_{eq} tends to have a small value in row ρ. The overall k_{eq} values monotonously increase with the increase in ρ, eventually saturating at 0.09. In contrast to γ_{eq}, the minimum k_{eq} values are located at the resonances, implying that the stiffening effect develops proportionally to the increase in ρ.

4 Conclusions

An ROM technique is proposed to examine the dynamic response of a frictionally constrained joint under cyclic loading. The proposed technique was developed based on the equivalent linearization of the nonlinear characteristics of the friction force at a joint interface. The key feature of the proposed approach is the quasi-static computation of the equivalent damping and stiffness values with the imposed harmonic

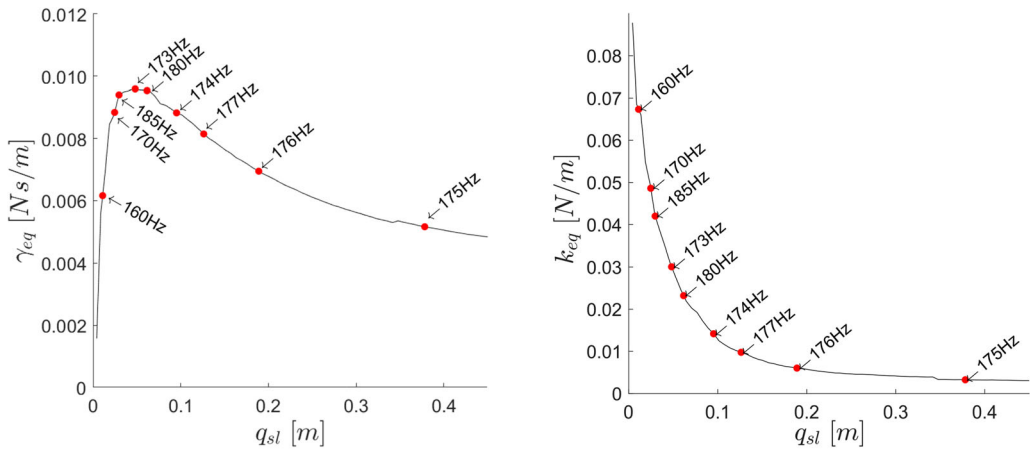

(a) Equivalent damping γ_{eq} (b) Equivalent stiffness k_{eq}

Fig. 12 Solution values of **a** equivalent damping **b** equivalent stiffness in the ROM at each excitation frequency, where $\rho = 0.8$

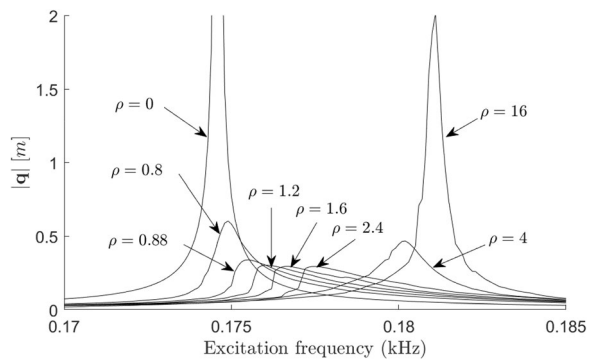

Fig. 13 Frequency responses, across for different ρ values

motion. The predictions of the friction-force-associated dynamic terms by adopting quasi-static results are validated based on the observations from this study. Equations 5 and 8 show that the energy dissipation and average stored energy during an excitation cycle in the modal domain were modal amplitude dependent. This finding was examined by comparing the resulting friction force numerically obtained from the quasi-static and time-domain analyses. Discrepancies in contact force propagations between the quasi-static results and the time domain results were observed; however, the resulting energy dissipation and average stored energy obtained from two different analyses were similar. Accordingly, the equivalent scheme for damping and stiffness was approximated by the quasi-static results. In turn, the precalculated equivalent damping and stiffness reduced the iteration costs for the ROM solution.

Another advantage of the proposed ROM technique is the prediction accuracy because the nonlinear friction force was obtained via the FE model. The results exhibited good accuracy with considerably reduced computational costs. Forced response computations were performed under various joint contact and loading conditions. The forced response results presented typical response transitions exhibiting the stiffening effect.

Unlike other approaches(Long and Tiso 2016; Witteveen and Fischer 2014; Pischler et al. 2017, 2017), this study does not provide a direct assessment of the nonlinear force at the contact interfaces. Instead, the proposed technique helps obtain the exact friction force quasi-statically via an FE analysis and parameterizes it into an equivalent format. As the ROM technique entails an exceedingly small (2×2), it significantly reduces the computation time for the predictions of the response amplitudes at

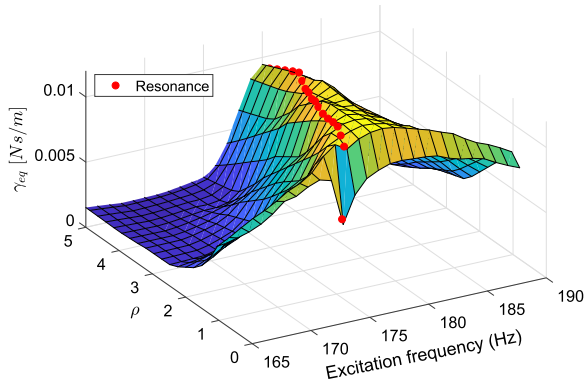

(a) Equivalent damping γ_{eq}

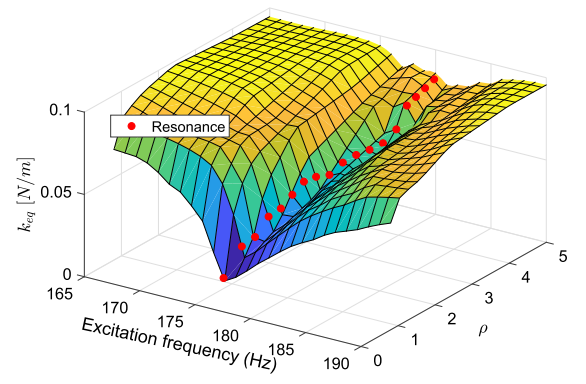

(b) Equivalent stiffness k_{eq}

Fig. 14 Predicted γ_{eq} and k_{eq} values for $165Hz \leq f_{ex} \leq 190Hz$ and $0.8 \leq \rho \leq 5$

the steady state. One important area for future development is to extend the proposed ROM technique to applications involving complex geometries.

Acknowledgements This work was supported by the National Research Foundation of Korea(NRF) grant funded by the Korea government(MSIT) (No. 2021R1F1A1052123).

Appendix A: Fixed point iteration convergence condition

The following theorem satisfies the conditions for the existence of a fixed point.

Theorem 1 Assume that $g \in \mathbf{C}[a,\ b]$, that is, $g(q)$ is continuous on the interval $[a,\ b]$. Thus, we arrive at the following conclusions:

1. If the range $y = g(q)$ ensures that y takes values in $[a,\ b]\ \forall q \in [a,\ b]$, then g has a fixed point in $[a,\ b]$.
2. Further, suppose that $g'(q)$ is defined in a range $(a,\ b)$ and that a constant $0 < \alpha < 1$ exists with $|g'(q)| \leq \alpha\ \forall x \in (a,\ b)$, then g possesses a unique fixed point $\bar{q}$ in $[a,\ b]$.

Appendix B: Solution convergence of Eq. (16)

The nonlinearity of Eq. (16) only exists in the values of $\gamma_{eq}(q)$ and $k_{eq}(q)$. The equivalent stiffness, shown in Fig. 15b, strictly decreases as q increases; however, the equivalent damping γ_{eq} increases monotonically until it reaches its peak value $(q^* \approx 0.05)$ and then decreases monotonically. Thus, we can divide three different regimes of the characteristics of nonlinearities as follows:

1. $0 < q < q^*$: monotonic increase of γ_{eq} and strict decrease of k_{eq}
2. $q \approx q^*$: near peak value of γ_{eq}
3. $q^* < q$: monotonic decrease of γ_{eq} and strict decrease of k_{eq}

The solution of Eq. (16) at a given excitation frequency falls into one of three criteria. We rewrite the Eq. (17), in the form

$$g(q) = \Theta(q)\mathrm{f}, \tag{19}$$

and examine the convergence of each criterion. In Fig. 15, the selected frequencies for each criterion are presented. The function $g(q)$ for each excitation is plotted in Fig. 16]. Recall from 1, $g(q)$ is continuous in

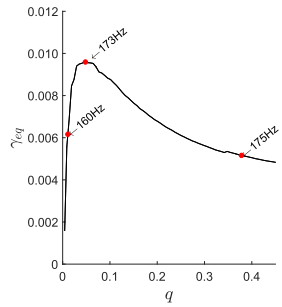

(a) Equivalent damping

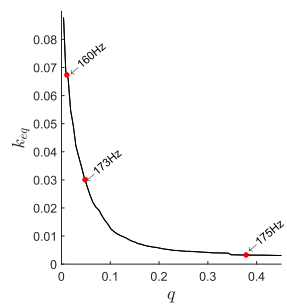

(b) Equivalent stiffness

Fig. 15 Equivalent damping and stiffness at $f_{ex} = 160Hz$, $f_{ex} = 173Hz$, and $f_{ex} = 175Hz$

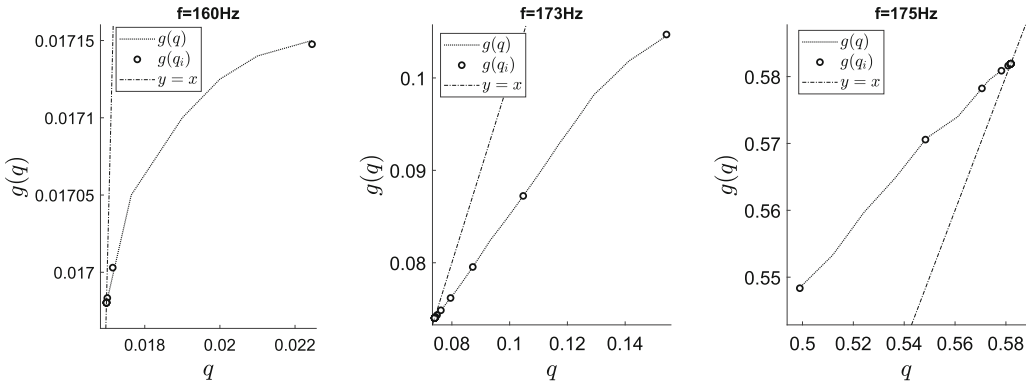

(a) $f_{ex} = 160Hz$ (b) $f_{ex} = 173Hz$ (c) $f_{ex} = 175Hz$

Fig. 16 The graph of $g(q)$, $y = x$ and iterative solutions of $q_{i+1} = g(q_i)$, $(i = 1, 2, 3, ...)$

the mapping range that agrees with the existence of a fixed point in the range of q (Theorem 1.1). Moreover, the slope of $g(q)$ is always less than 1 $(y = x)$, which satisfies Theorem 1.2. This implies that Eq. (16) permits a unique fixed point.

References

Ahmadian, H., Jalali, H.: Generic element formulation for modelling bolted lap joints. Mech. Syst. Signal Process. **21**, 2318–2334 (2007)

Allara, M.: A model for the characterization of friction contacts in turbine blades. J. Sound Vib. **320**, 527–544 (2009)

Areias, P., Queirós de Melo, F., Carrilho Lopes, J.: Combined sticking: a new approach for finite-amplitude Coulomb frictional contact, International Journal of Mechanics and Materials in Design, 16, 619-631 (2020)

Baek, Seunghun., Epureanu, Bogdan. I.: Reduced-Order Modeling of Bladed Disks With Friction Ring Dampers, Journal of Vibration and Acoustics, 139, 061011-061011-9 (2017)

Bathe, K.J., Gracewski, S.: On nonlinear dynamics analysis using substructuring and mode superposition. Computer and structures **13**, 699–707 (1981)

Beards, C.F.: The damping of structural vibration by controlled inter-facial slip in joints. J. Vib. Acoust. Stress. Reliab. Des. **105**, 369–373 (1983)

Beards, C.F.: The damping of structural vibration by controlled interfacial slip in joints. J. Vib. Acoust. Stress. Reliab. Des. **105**, 369–373 (1983)

Beucke, K.E., Kelly, J.M.: Equivalent linearizations for practical hysteretic systems. Int. J. Non-linear Mech. **20**(4), 211–238 (1985)

Chen, J. J., Menq, C. H.: Prediction of the resonant response of frictionally constrained blade systems using constrained mode shapes, Turbo Expo: Power for Land, Sea, and Air, 5 (1998)

Dossogne, T., Jerome, T. W., Lancereau, D. P. T., Smith, S. A., Brake, M. R. W., Pacini, B. R., Reuβ, P., Schwingshackl, C. W.: Experimental assessment of the influence of interface geometries on structrual dynamic response, Dynamics of Coupled Structures, Conference Proceedings of the Society for Experimental Mechanics Series, 4, 255-261 (2017)

Earles, S.W.E.: Theoretical estimation of the frictional energy dissipation in a simple lap joint. J. Mech. Eng. Sci. **8**, 207–214 (1966)

Eaton, D. C. G., Mead, D. J.: Interfacial damping at riveted joints, U.S.A.A. Report No. 241 (University of Southampton) (1963)

Ferri, A.A.: Friction damping and isolation systems. J. Vib. Acoust. **117**, 196–206 (1995)

Gaul, L., Nitsche, R.: The role of friction in mechanical joints. ASME. Appl. Mech. Rev. **54**, 93–106 (2001)

Den Hartog, J.P.: LXXIII. Forced vibrations with combined viscous and coulomb damping. The London, Edinburgh, Dublin Philos. Mag. J. Sci. **9**, 801–817 (1930)

Kim, J.H., Jang, Y.H.: Frictional Hertzian contact problems under cyclic loading using static reduction. Int J Solids Struct **51**, 252–258 (2014)

Kim, J.H., Jang, Y.H.: Frictional contact behaviors between beam and cylinder under cyclic loading. Int J Mech Sci **131–132**, 693–700 (2017)

Lacayo, R., Pesaresi, L. Johann G., Fochler, D., Armand, J., Salles, L., Schwingshackl, C., Allen, M., Brake, M.,: Nonlinear modeling of structures with bolted joints: A comparision of two approaches based on a time-domain and frequency-domain solver. Mech. Syst. Signal Process. **114**, 413–438 (2019)

Lotstedt, Per: Mechanical systems of rigid bodies subject to unilateral constraints. SIAM J. Appl. Math. **42**, 281–296 (1982)

Mead, D. J., Eaton, D. C. G.: Interfacial damping at riveted joints, U.S.A.A. Report No. 153 (University of Southampton) (1960)

Miller, R.K.: The steady state response of systems with hardening hysteresis. J. Mech. Des. **100**, 193–198 (1977)

Nickell, R.E.: Nonlinear dynamics by mode superposition. Comput. Methods Appl. Mech. Eng. **7**, 107–129 (1976)

Noor, A.K.: Recent advances in reduction method for nonlinear problems. Comput. Struct. **13**, 31–44 (1981)

Petrov, E.P., Ewins, D.J.: Analytical formulation of friction interface elements for analysis of nonlinear multiharmonic vibrations of bladed discs. Trans. ASME J. Turbomach. **215**(2), 364–371 (2003)

Pfeiffer, F.: Dynamical systems with time-varying or unsteady structure. Gesellschaft fuer angewandte Mathematik und Mechanik, Wissenschaftliche Jahrestagung, Hanover, Federal Republic of Germany **71**, T6–T22 (1991)

Pfeiffer, F.: Dynamical systems with unsteady processes, The. Am. Soc. Mech. Eng. **49**, 65–74 (1992)

Pischler, F., Witteveen, W., Fischer, P: A complete strategy for efficient and accurate multibody dynamics of flexible structures with large lap joints considering contact and friction. Multibody Syst. Dyn. **40**, 407–436 (2017)

Pischler, F., Witteveen, W., Fischer, P.: Reduced-order modeling of preloaded bolted structures in multibody systems by the use of trial vector derivatives. J. Comput. Nonlinear Dyn. **12**, 051032-051032–12 (2017)

Ren, Y., Lim, T.M., Lim, M.K.: Identification of properties of nonlinear joints using dynamic test data. J. Vib. Acoust. **120**, 324–330 (2008)

Sabelkin, V., Mall, S.: Investigation into cylinder-on-flat adhesion elastic-plastic micro-contact under repeated loading and unloading condition. Int. J. Mech. Mater. Des. **3**, 373–388 (2006)

Slaats, P.M.A., Jongh, J., Sauren, A.A.H.J.: Model reduction tools for nonlinear structural dynamics. Comput. Struct. **54**, 1155–1171 (1995)

Tang, W., Baek, S., Epureanu, B.I.: Reduced-order models for blisks with small and large mistuning and friction dampers. J Eng Gas Turbines Power **139**, 012507-1-7–13 (2017)

Tang, W., Epureanu, B.I.: Geometric optimization of dry friction ring dampers. Int. J. Non-linear Mech. **109**, 40–49 (2019)

Thaitirarot, A., Hills, D.A., Dini, D.: Contact mechanics of frictional lap joints. J. Strain Anal. Eng. Des. **48**, 321–329 (2013)

Witteveen, W., Fischer, P.: Efficient Model Order Reduction for the Dynamics of Nonlinear Multilayer Sheet Structures with Trial Vector Derivatives, Shock and Vibration, 2014, 16 pages (2014)

Wu, L., Tiso, P: Nonlinear model order reduction for flexible multibody dynamics: a model derivatives approach. Multibody Sys. Dyn. **36**, 405–425 (2016)